



Dose measurements in a thorax phantom at 3DCRT breast radiation therapy

Elsa Bifano Pimenta¹, Luciana Batista Nogueira², Tarcísio Passos Ribeiro de Campos¹

¹Department of Nuclear Engineering, Federal University of Minas Gerais, Belo Horizonte, Brazil

²Department of Anatomy and Image, Federal University of Minas Gerais, Belo Horizonte, Brazil

ABSTRACT

Background: The anthropomorphic and anthropometric phantom developed by the research group NRI (Núcleo de Radiações Ionizantes) can reproduce the effects of the interactions of radiation occurring in the human body. The whole internal radiation transport phenomena can be depicted by film dosimeters in breast RT. Our goal was to provide a dosimetric comparison of a radiation therapy (RT) plan in a 4MV 3D-conformal RT (4MV-3DCRT) and experimental data measured in a breast phantom.

Materials and methods: The RT modality was two parallel opposing fields for the left breast with a prescribed dose of 2.0 Gy in 25 fractions. The therapy planning system (TPS) was performed on CAT3D software. The dose readings at points of interest (POI) pre-established in TPS were recorded. An anthropometric thorax-phantom with removal breast was used. EBT2 radiochromic films were inserted into the ipsilateral breast, contralateral breast, lungs, heart and skin. The irradiation was carried out on 4/80 Varian linear accelerator at 4MV.

Results: The mean dose at the OAR's presented statistically significant differences ($p < 0.001$) of 34.24%, 37.96% and 63.47% for ipsilateral lung, contralateral lung, and heart, respectively. The films placed at the skin-surface interface in the ipsilateral breast also showed statistically significant differences ($p < 0.001$) of 16.43%, -10.16%, -14.79% and 15.67% in the four quadrants, respectively. In contrast, the PTV dosimeters, representative of the left breast volume, encompassed by the electronic equilibrium, presented a non-significant difference with TPS, $p = 0.20$ and $p = 0.90$.

Conclusion: There was a non-significant difference of doses in PTV with electronic equilibrium; although no match is achieved outside electronic equilibrium.

Key words: radiochromic film; breast cancer; thorax phantom

Rep Pract Oncol Radiother 2021;26(2):242-250

Introduction

Treatment planning systems (TPS) are software tools used for external radiotherapy. TPS predicts dose distributions and generates beam shapes allowing the optimization of the tumor control probability (TCP) and the reduction of the likelihood of normal tissue complications (NTCP) [1].

Meanwhile, most TPSs present some limitations in predicting superficial doses in the skin, in interfaces of heterogeneous materials, in the voids, and low density regions such as the lungs [1, 2]. Radiotherapy of breast cancer involves a complex anatomy and various tissues of highly different densities, including soft tissue, lung, bone, and air [3]. Unlike acrylic phantoms, the anthropomorphic and

Address for correspondence: Elsa Bifano Pimenta, Department of Nuclear Engineering, Federal University of Minas Gerais, Belo Horizonte, MG 31270-901, Brazil; e-mail: elsabpimenta@gmail.com

This article is available in open access under Creative Common Attribution-Non-Commercial-No Derivatives 4.0 International (CC BY-NC-ND 4.0) license, allowing to download articles and share them with others as long as they credit the authors and the publisher, but without permission to change them in any way or use them commercially

anthropometric phantom developed by the NRI (Núcleo de Radiações Ionizantes) research group from UFMG can reproduce the effects of the interactions of radiation with the human body. Briefly, this thorax phantom contains the synthetic heart, lungs, and spinal cord similar in density to their human counterparts, mimicking heterogeneous thoracic anatomy [4].

Electronic equilibrium occurs when scattering secondary electrons from primary photon radiation achieves paths with the angular isotropic distribution. Such conditions have been studied in homogeneous water medium exposed by energetic photons in which Compton scattering is a predominant process [5]. Besides, an inhomogeneous medium causes electronic disequilibrium and reduction of absorbed energy in regions close to the inhomogeneity materials. Such longitudinal electron disequilibrium results in a build-up region. The effect of the build-up occurs when the beam passes from a lower density to a higher density medium, and the re-build-up occurs in the reverse direction, from the highest to the lowest density [6, 7]. On the TPS, dose calibration occurs only in a homogeneous medium in which electronic equilibrium condition is held. Herein, dose is defined as absorbed energy per specific mass. The TPS dose calculation in the build-up region is estimated from the data's extrapolation measured on the basis of the maximum dose depth using adjusted functions [8].

In the case of high energy photons in low density material or in small beam's portals, the lateral electron path can be larger than the field size and, thus, lateral electron disequilibrium (LED) can occur. In the low density lung tissue, the dose from scattered electrons is deposited further away from the interaction points, far from than the correction algorithm predicts. Therefore, the dose is overestimated in the high dose region (infield) and underestimated in the low dose region of the lung, outside the radiation field [3]. The effects of LED on the lung dose are generally poorly accounted for by commercial dose calculation algorithms which oversimplify the secondary electron trajectory [9–15].

In addition, the surface dose can be influenced by the contamination of electrons from the collimator system, by the secondary scattering photons of the gantry and also by backscattering photons from the underlying tissue layers, mainly unpredictable by TPS [16]. Most of the commercially available

TPS calculate the exit dose under the full scatter conditions and cannot accurately provide the entrance skin doses [8].

Therefore, the reproduction of the internal dosimetry through detectors in phantoms may increase the knowledge of the effects of the interaction of radiation on the human being in radiotherapy, especially in heterogeneous interfaces, skin surface and low density material, as present in breast radiation therapy where electronic disequilibrium persists.

The goal was to provide a 4MV-3DCRT dosimetry in a realistic breast thorax phantom, investigating especially the inhomogeneous organs interfaces and skin, regions with non-electronic equilibrium, matching values with TPS for the propose of adopting anthropomorphic and anthropometric phantoms in a clinical routine.

Materials and methods

The 3D-CRT therapy plan

The plan was performed in the CAT3D TPS, from Mevis Medical Company, supported by the Pencil Beam Convolution algorithm. The chosen modality was the three-dimensional conformal RT (3D-CRT) based on two parallel opposite fields applied in the ipsilateral breast exposure of an anthropometric and anthropomorphic thorax phantom with a prescribed dose of 2.0 Gy in 25 fractions. The planning target volume (PTV) and the following organs at risk (OAR) were selected: lungs, heart, and contralateral breast.

The planning was optimized matching the combination of two weighted modulated irradiation fields in which monitor units (MU) associated with each field, collimator, gantry and angular positions were set. A suitable planning conformation was proposed, covering the whole PTV, and minimizing the exposure of the OAR's. The secondary collimators known as jaws determine the size of the field. The wedges were set in order to modify the dose distributions. A 15° wedge filter was used for each field to avoid beam divergence, as shown in Table 1.

Preparation of anthropomorphic and anthropomorphic breast phantom

A thorax phantom was previously prepared, as described by Schettini et al. 2007 [17]. Some adjustments were adopted, including the skin, heart and muscle manufactured. Breasts were fabricated and

Table 1. Radiotherapy protocol of the 3D-conformal radiotherapy (3DCRT)

Parameters	ML Field ^a	LM Field ^a
Isocenter	Iso	Iso
Field X	160	160
Field Y	100	100
Table Ang	0	0
Gantry Ang	233	48
Gantry Rot	0	0
Collim Ang	11	350
Weight	1.1	1
Wedge Filtr	W15	W15
Wedge Pos	CCW	CW
Tray Factor	1	1
Head-jaw	0	0
Feet-jaw	0	0
Right-jaw	0	0
Left-jaw	0	0
SSD	727.6	725.6
Device	0	0
MU	145.0	134.8

SSD — source to surface distance; MU — monitor unit

adapted to the thorax phantom. The proportion of glandular tissue and adipose tissue of the breasts was 50:50 to represent a fibroadipose breast. The glandular tissue was made of a natural elastomer in the weight percentage of 77%, including 10% graphite powder, 0.3% NH₄Cl (0.1%), NH₄ (4.1 g) present in the elastomer, (NH₄)₂SO₄ (0.9%), NH₄H₂PO₄ (0.18%), C₂₈H₃₀Na₈O₂₇ (0.3%), NaH₂PO₄ (0.3%), KC (0.2%), H₂O (7.7%) present in the elastomer, NaCl (0.08%). After drying, the tissue lost 15% in weight, already considered in its elementary chemical composition. The chemical elements constitution of glandular TE achieved were: carbon (78.0%), hydrogen (10.9%), oxygen (7.6%), nitrogen (3.4%), sodium (0.1%), phosphorus (0.1%), sulfur (0.2%), chlorine (0.2%) and potassium (0.1%), based on stoichiometric calculations using the constituent compounds.

The adipose tissue surrounding the breast was manufactured with 30% paraffin, 25% carnauba wax and 45% polyol mineral oil. The thorax muscle tissue and the heart were fabricated with the same material as the glandular tissue; however, with small differences in proportion to match the elementary chemical composition of the heart tissues in mass weight.

For the manufacture of skin tissue, 50% animal collagen gelatin and 50% hydraulic silicone were mixed [18]. The ribs and spine were made of animal bone powder, washed, dried, sieved, sterilized, glued with orthophthalic resin. The similarity of the elementary chemical composition, number of Hounsfield, and coefficients of conversion of fluency-Kerma to photons and neutrons were verified for each organ of the phantom, already documented in literature [17].

Phantom and dosimeter positioning

EBT2 radiochromic films of 3 × 2 cm² were placed in each quadrant of the skin of the ipsilateral breast, where the films, coded as BS1, BS2, BS3 and BS4, were placed in the upper medial, upper lateral, lower lateral and lower medial quadrant, respectively, as shown in Figure 1A. The measurements in OARs were performed by inserting into the ipsilateral breast, contralateral breast, lungs, and heart in the coronal axis as in the scheme shown in Figure 1B. The absorbed dose in PTV was measured with four M1, M2, M3 and M4 films of different sizes due to the anatomical shape of the breast. They were inserted into the ipsilateral breast of the thorax phantom (Fig. 1C), along the axial axis, as shown in Figure 1D.

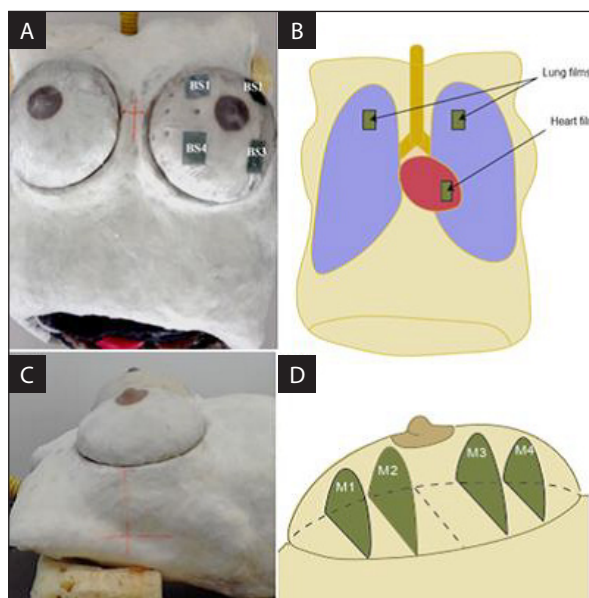


Figure 1. The films BS1, BS2, BS3 and BS4 placed in each quadrant on ipsilateral breast skin (A). The organ at risk (OAR) films were inserted in the two lungs and in the heart myocardium (B). The planning target volume (PTV) films (M1, M2, M3 and M4) were inserted into the ipsilateral breast of thorax phantom (C) along the axial axis (D)

Irradiation on LINAC

The irradiation was performed on the Varian model 4/80 Varian linear accelerator at 4MV spectrum, made available from the Institute of General Radiotherapy and Megavoltage of Minas Gerais, Brazil.

Dose versus optical density correlation

Calibration was performed in a water-tank phantom at 100 cm SSD, holding a set of films in depth ranging from 1.5 cm to 19.5 cm with increments of 2.0 cm. The film's response was correlated with absorbed dose measured in a secondary standard ionizing chamber dosimeter, placed in the same depth in the same water tank phantom. The dose interval was 0 to 4.0 Gy. The calibration films were digitized in the transmission mode scanner.

The optical densities (OD) of the red (R) component of the set of digitized films were generated. A correlation between doses as a function of OD was achieved adjusting the data. The following polynomial function was obtained empirically based on Beer-Lambert's law [19]:

$$y = A.OD + B.OD^n \quad (1)$$

in which the coefficients A and B are estimated from the experimental data correlating the absorbed dose (y) as a function of the OD, where n is the degree of the polynomial function.

Dose analysis and intercomparison

All M1 to M4 and BS1 to BS4 dosimeters were digitized and an HP Scanjet G4050 scanner. The RGB components were split and R-component image treated. Optical density was evaluated in the R-component image on a pixel basis. Based on Eq. 1, dose distribution was generated on the images, sup-

ported by the ImageJ software. The absolute mean doses and standard deviation of the data from films present on the PTV and OAR were evaluated. For the dosimetric intercomparison, a CAT3D tool, namely POI, was used. It allowed the reading of the absolute dose at points of interest (POI) pre-established in the TPS. This tool is usually used to define the isocenter of the PTV.

The calibration radiochromic conditions were at the same as those for the LINAC dose calibration, with a similar temperature and pressure environment. The calibration curve was fed with similar dose data as the TPS.

Statistical analysis

Student t-test with the significance level of 5% was used to compare the means of the doses from the radiochromic films with the mean values in the POIs from TPS.

Results

The therapy plan

Figure 2 depicts the CT images of the phantom and the plan adopted for this dosimetric study, provided by the CAT3D MEVIS Medical Company.

Dose versus optical density response

The parameters found in the calibration curve of the films were $a = 5.57 \pm 3.39$; $b = 91.47 \pm 94.16$; $n = 2.57 \pm 0.93$ with a coefficient of determination of 0.998.

Internal phantom dosimetry compared to TPS

Figure 3 depicts the spatial dose maps generated in M1, M2, M3 and M4 films of the internal

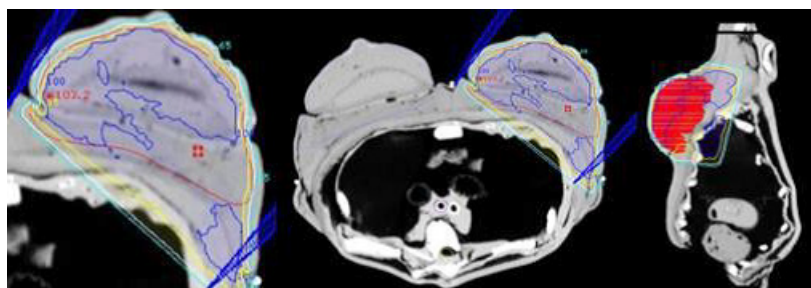


Figure 2. The 3D-conformal radiotherapy (3D-CRT) plan performed in CAT3D based on axial images registered by the CT. Images were superposed to the axial CT image sections, and a sagittal reconstruction was performed

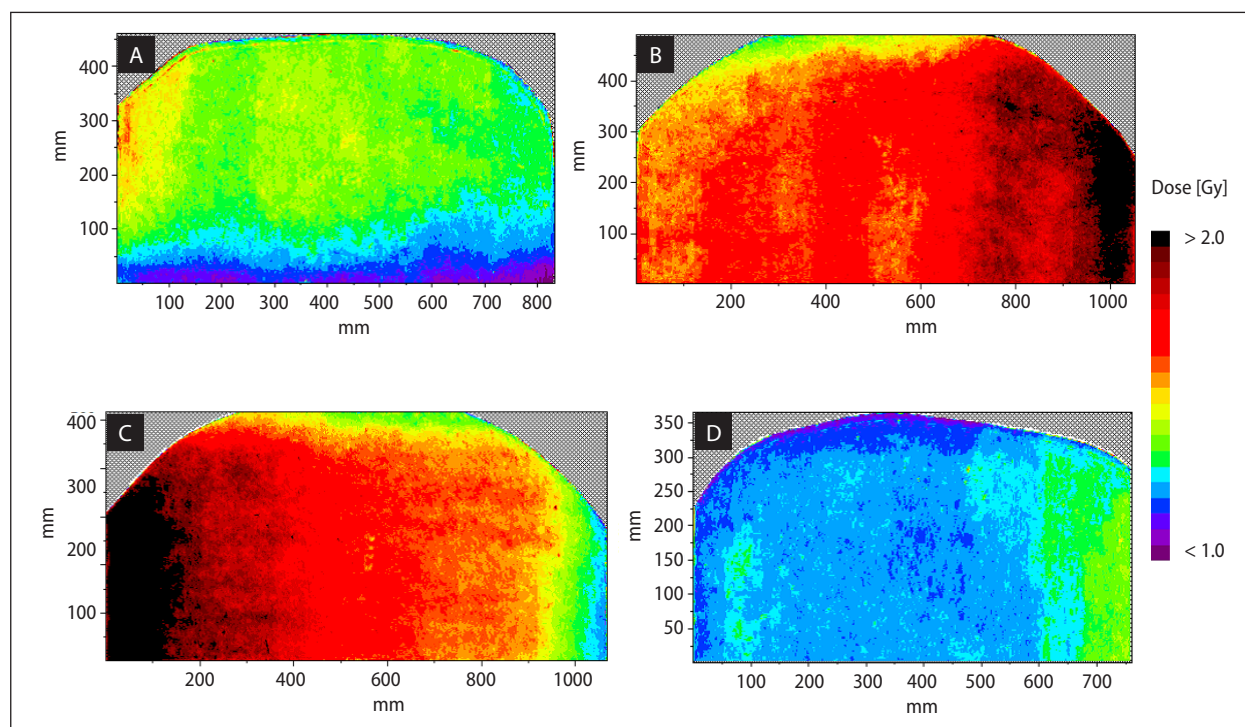


Figure 3. Spatial dose maps generated within M1 (A), M2 (B), M3 (C) and M4 (D) dosimeters placed in the left-breast exposed with the 3D-conformal radiotherapy (3D-CRT), in which XY-scales were in mm and dose scale in Gy

Table 2. Comparison of EBT2 film and CAT3D

Films	Dose Film [Gy]	Dose TPS [Gy]	Difference (%)
M1	1.31 ± 0.11	2.04 ± 0.05	-55.35 ($p < 0.001$)
M2	1.95 ± 0.17	2.05 ± 0.21	-5.17 ($p = 0.20$)
M3	1.93 ± 0.17	2.02 ± 0.84	-4.38 ($p = 0.90$)
M4	1.16 ± 0.10	1.99 ± 0.07	-71.35 ($p < 0.001$)
Ipsilateral lung	0.30 ± 0.03	0.20 ± 0.22	34.24 ($p < 0.001$)
Contralateral lung	0.03 ± 0.00	0.02 ± 0.00	37.95 ($p < 0.001$)
Heart (myocardium)	0.26 ± 0.02	0.09 ± 0.02	63.47 ($p < 0.001$)
BS1	1.12 ± 0.10	0.94 ± 0.66	16.43 ($p < 0.001$)
BS2	1.13 ± 0.10	1.24 ± 0.5	-10.16 ($p = 0.10$)
BS3	1.18 ± 0.10	1.35 ± 0.68	-14.79 ($p < 0.001$)
BS4	0.95 ± 0.08	0.8 ± 0.15	15.67 ($p < 0.001$)

left-breast exposed with 3D-CRT. Table 2 shows the doses in the dosimeters in the breast.

Discussion

The ideal equation for the calibration curve is still questionable, but a second or higher order polynomial is often used in adjusting the calibration equation based on Taylor's theorem [20–23]. In our case, the coefficient of determination of 0.998 provided

a suitable value which guarantees a well-adjusted mathematical representation of the data. This was consistent with Silva et al. (2018) which has found n equal to 2.5 for both water and solid water in the range of 50–450 cGy with 4 MV Varian's Clinac 6XSN11 [26].

The film calibration was performed in water since this material is the recommended reference standard for the determination of absorbed dose in the IAEA document TRS 398 [24]. According to

TRS 398, this material is the most similar to the human tissue composition for photons. Thus, it is expected that the absorption and scattering properties of radiation are equivalent [25, 26]. The calculation tables often used in dose calibration in radiotherapy centers, which are the same for clinical cases, are prepared in water.

The calibration curve was built based upon the relationship between the dose and the optical density of the film in an equilibrium electronic condition. Indeed, it captured the relationship between the amount of organic chemical reactions that produce color on the film to the concentration of secondary electrons and free radicals induced by radiation exposure in the film. Hence, regardless of the distinct phenomenon of secondary electron and photon interactions in a medium or interfaces, the correlation between chemical reactions and free radicals is preserved. Nevertheless, the chemical reaction rate is energy-dependent, which explains a slight variation of the radiochromic color density with the incident particle energy. Although the radiation intensities are distinct in the phantom and in the calibration tank of water, their internal energy spectra were provided by the same LINAC radiation source; therefore, the energy-dependence may be negligible.

After TPS was installed, commissioning and modeling were carried out. Commissioning was done for various dose measurements in water-tank phantom at various depths, LINAC's energies, and field sizes. These measurements were converted into tables, and those values were recorded in TPS, called modeling tables. In addition, a secondary water-dosimetry is performed monthly using the data in the table to check the dose and TPR_{20/10}. In this way, our radiochromic-film-based dosimeter was validated with the doses in the TPS, since both used the same secondary water dosimetry and water-tank phantom. Those experiments were performed at the time of the LINAC calibration data, under similar temperature and pressure conditions.

The breast phantom anatomy, especially the chest wall thickness, and the uncertain positioning in the detector relative to the breast surface and thorax, among other factors, influenced the dose measurements and its comparison to TPS. Whereas the maximum dose depth for a 4MV photon beam is 1.0 cm, the M1 and M4 films positioned near the breast surface in the equivalent adipose tissue were

encompassed by the build-up region; therefore, TPS could not predict dose well in a non-electronic equilibrium environment.

Table 2 summarizes the comparison of radiochromic film and TPS based pencil beam algorithm. The dose in the build-up region close to the skin was not accurately considered by the TPS, justifying the low average doses provided by the PTV in the positions of the M1 and M4 films, since those films were placed around the breast surface, enclosed in the build-up region. In addition, the same can be said for the high percentage differences in ipsilateral breast skin whose values were within $\pm 20\%$.

The mean doses of M2 and M3 films in PTV were within the recommendations of the ICRU report No. 50, where the absorbed dose delivered cannot vary more than $\pm 5\%$ with respect to the prescribed dose [27]; while the values of the M1 and M4 films near the surface were not in agreement. The differences between mean dose measurements in the phantom and found in the TPS were 4.91% and 4.20%. The t-test for dosimetric intercomparison of sections M2 and M3 showed a non-significant difference.

Nogueira et al. (2015) have measured the absorbed dose in 3D CRT left-breast radiation therapy in a sagittal film placed at the center of a synthetic breast [28]. Their RT-protocol followed the dose prescribed of 1.8 Gy in 28 fractions. The average dose per fraction at the sagittal dosimeter placed at the center of the breast was 1.9 ± 0.2 Gy, and the TPS was 1.84 ± 0.2 Gy at the same position [28]. Indeed, the dose distribution at the whole PTV varied from 100% up to 112% of the prescribed dose; while TPS provided 100% up to 105% [28]. Our experiment provided 96% of the prescribed dose at M2 and M3 dosimeters placed on the transverse plane inside the breast. In both experiments, the film positioning, the Linac-type and the TPS protocols were distinct; however, in the left-breast, inside the electronic equilibrium region, the doses were compatible with the prescribed dose. In the same experiment, the skin dose of the ipsilateral breast varies from 1.0 to 1.4 Gy, having an average dose of 1.20 ± 0.10 Gy [28]. In the ipsilateral breast skin, the dose achieved 1.10 ± 0.10 Gy, evaluated on three films placed on the breast-skin [29]. In our experiment, BS1 up to BS4 provided an average dose of 1.09 ± 0.09 Gy.

The percentage dose discrepancy on the heart can be explained by the heterogeneity of the lung. The radiochromic film might have detected a build-up region, possibly present in the lung-heart interface due to its 0.3/1.05 density ratio, while the TPS's are known to be inaccurate in regions outside the electronic unbalance such as build-up regions. The non-reproducibility of the heart positioning in the phantom may also have contributed to the percentage difference, since the distance between the heart and the radiation field may have been altered after the insertion of the films. The percentage differences in lung dose can be explained by the difficulty of TPS (in this case, Pencil Beam) to accurately predict the variations of the local electron density of the lung and, therefore, adequately respond to the effects of electronic lateral scattering and re-build-up.

It has been observed that the main limitations in the experimental dose measurements in the phantom are due to anatomic discrepancies with human beings. Indeed, the tomographic representation used in TPS was the same as in the physical phantom. Thus, the same anatomic discrepancies were reproduced on the TPS. The build-up region in the skin-interface can be addressed in the physical phantom and in its modelling feed in the TPS. Despite the dosimetric correlation, a comparison to a human being dosimetry cannot be called, especially near the regions that have an anatomical discrepancy with human anatomy.

Despite the anatomic discrepancies and positioning errors of the phantom, the limitations of the dose calculations of the TPS software persist in the heterogeneous interfaces, skin surface and low-density material, often present in breast radiation therapy. Such limitations showed up also in the tomographic-phantom modelling used in the TPS. Lack of electronic disequilibrium persists, and it was responsible for the overall differences between dose predicted by a TPS and measured values in the phantom. The overall responses of several well-known therapy planning systems (TPS) have been investigated in literature [30], with distinct complexity and modeling heterogeneity, doses in blocked regions, or tangential effects. According to the IAEA pilot study, CAT3D TPS is among the most accurate systems available on the market. EBT2 films present limitations, especially in calibration procedures; however, there

are recommendations in its use in quality assurance in radiation therapy where dose uncertainty of up to 2.8% is acceptable [31]. We found that EBT2 dosimeter is a suitable tool for reproducing normalized spatial dose distribution into anthropometric and anthropomorphic phantoms, to study heterogeneity among other conditions. In the present paper, the dosimeter was able to capture internal build-up phenomena in 3DCRT breast radiation therapy.

In summary, our findings were experimental mean doses in M2 and M3 films to the PTV in agreement with TPS, while discrepancy values of the M1 and M4 films at the PTV but near the skin-surface. Experimental overdose of 34.24%, 37.96% and 63.47% for the ipsilateral lung, contralateral lung, and heart, respectively, 15% to the skin at the internal right side of the breast, and 10% sub dose outside. Such values demonstrated poor dose predictions of the pencil beam convolution algorithm calculation in sites of non-electronic equilibrium environment.

The measurement of doses in phantoms can provide much information about the interactions of the radiation with tissues. Film detectors may contribute to recording such data. The intercomparison with TPS is a challenge since there are large uncertainties in film positioning, calibration processes, and absence of precise reference points.

Conclusions

Dosimetry, including a realistic breast phantom, was a useful tool to record phenomena such as build-up, re-build-up, electronic side balance and electronic contamination, complementing the information of the TPS by depicting doses in regions where those calculated values are imprecise, as in the skin dose and organ interfaces with high heterogeneity. Indeed, our findings show statistically non-significant difference between the electronic-equilibrium PTV regions and the experimental and TPS values. However, for near heart-lung interfaces, discrepancies were up to 40%. Skin measured doses matched with values found in literature, with $\pm 20\%$ of TPS data. Therefore, there are no robust protocols that can establish quality control of the internal dose in overall regions of the patients. Our findings support the adoption of an anthropomorphic and anthropometric phantom as a tool to

help physicists carry out a more comprehensive QA program routine.

Conflict of interests

The authors declare that there is no conflict of interests regarding the publication of this paper.

Funding

None declared.

Acknowledgments

The authors express their gratitude to the medical physicist Sávio F. Rosa for his support and assistance in experimental support. In addition, we express our gratitude to the Institute of General Radiotherapy and Megavoltage of Minas Gerais for providing the facility, and CNEN for financial support with a master's degree scholarship. We thank MEVIS Medical Company for all the technical support and availability of the planning software, which has been useful in learning and research in the field of radiotherapy. We are thankful to CNPq, REBRAT-SUS project.

References

- Elcim Y, Dirican B, Yavas O. Dosimetric comparison of pencil beam and Monte Carlo algorithms in conformal lung radiotherapy. *J Appl Clin Med Phys*. 2018; 19(5): 616–624, doi: [10.1002/acm2.12426](https://doi.org/10.1002/acm2.12426), indexed in Pubmed: [30079474](https://pubmed.ncbi.nlm.nih.gov/30079474/).
- Akbaş U. Investigation of Surface Dose Using Film Dosimetry and Commercial Treatment Planning System for Larynx Cancer Treatment with Intensity-Modulated Radiotherapy and Volumetric Modulated Arc Therapy. *Turk Onkoloji Dergisi*. 2018; 33(1), doi: [10.5505/tjo.2018.1736](https://doi.org/10.5505/tjo.2018.1736).
- Hedin E, Bäck A, Chakarova R. Impact of lung density on the lung dose estimation for radiotherapy of breast cancer. *Phys Imag Radiat Oncol*. 2017; 3: 5–10, doi: [10.1016/j.phro.2017.07.001](https://doi.org/10.1016/j.phro.2017.07.001).
- Anthropomorphic and anthropometric simulators of the structures, tissues and organs of the human body, by Campos, T.P.R. Thompson, L. Nogueira, L.B. Duarte, I.L. Matos, C.H. Teixeira, A.S. Maia, M. Schettini, M.P. Toledo, J.M (2012, May). Patent PI1004465- 004465.
- Nizin PS. Electronic equilibrium and primary dose in collimated photon beams. *Med Phys*. 1993; 20(6): 1721–1729, doi: [10.1118/1.596959](https://doi.org/10.1118/1.596959), indexed in Pubmed: [8309445](https://pubmed.ncbi.nlm.nih.gov/8309445/).
- Salata C, Sibata C, Ferreira N, et al. Computer simulation of a 6 MV photon beam in different heterogeneous media utilizing the PENELOPE code. *Radiol Bras*. 2009; 42(4): 249–253.
- Glide-Hurst CK, Chetty IJ. Improving radiotherapy planning, delivery accuracy, and normal tissue sparing using cutting edge technologies. *J Thorac Dis*. 2014; 6(4): 303–318, doi: [10.3978/j.issn.2072-1439.2013.11.10](https://doi.org/10.3978/j.issn.2072-1439.2013.11.10), indexed in Pubmed: [24688775](https://pubmed.ncbi.nlm.nih.gov/24688775/).
- Devic S, Seuntjens J, Abdel-Rahman W, et al. Accurate skin dose measurements using radiochromic film in clinical applications. *Med Phys*. 2006; 33(4): 1116–1124, doi: [10.1118/1.2179169](https://doi.org/10.1118/1.2179169), indexed in Pubmed: [16696489](https://pubmed.ncbi.nlm.nih.gov/16696489/).
- Disher B, Hajdok G, Gaede S, et al. Forcing lateral electron disequilibrium to spare lung tissue: a novel technique for stereotactic body radiation therapy of lung cancer. *Phys Med Biol*. 2013; 58(19): 6641–6662, doi: [10.1088/0031-9155/58/19/6641](https://doi.org/10.1088/0031-9155/58/19/6641), indexed in Pubmed: [24018569](https://pubmed.ncbi.nlm.nih.gov/24018569/).
- Aarup LR, Nahum AE, Zacharatou C, et al. The effect of different lung densities on the accuracy of various radiotherapy dose calculation methods: implications for tumour coverage. *Radiother Oncol*. 2009; 91(3): 405–414, doi: [10.1016/j.radonc.2009.01.008](https://doi.org/10.1016/j.radonc.2009.01.008), indexed in Pubmed: [19297051](https://pubmed.ncbi.nlm.nih.gov/19297051/).
- Chow JCL, Leung MKK, Van Dyk J. Variations of lung density and geometry on inhomogeneity correction algorithms: a Monte Carlo dosimetric evaluation. *Med Phys*. 2009; 36(8): 3619–3630, doi: [10.1118/1.3168966](https://doi.org/10.1118/1.3168966), indexed in Pubmed: [19746796](https://pubmed.ncbi.nlm.nih.gov/19746796/).
- Carrasco P, Jornet N, Duch MA, et al. Comparison of dose calculation algorithms in phantoms with lung equivalent heterogeneities under conditions of lateral electronic disequilibrium. *Med Phys*. 2004; 31(10): 2899–2911, doi: [10.1118/1.1788932](https://doi.org/10.1118/1.1788932), indexed in Pubmed: [15543799](https://pubmed.ncbi.nlm.nih.gov/15543799/).
- Jones AO, Das IJ. Comparison of inhomogeneity correction algorithms in small photon fields. *Med Phys*. 2005; 32(3): 766–776, doi: [10.1118/1.1861154](https://doi.org/10.1118/1.1861154), indexed in Pubmed: [15839349](https://pubmed.ncbi.nlm.nih.gov/15839349/).
- Knöös T, Wieslander E, Cozzi L, et al. Comparison of dose calculation algorithms for treatment planning in external photon beam therapy for clinical situations. *Phys Med Biol*. 2006; 51(22): 5785–5807, doi: [10.1088/0031-9155/51/22/005](https://doi.org/10.1088/0031-9155/51/22/005), indexed in Pubmed: [17068365](https://pubmed.ncbi.nlm.nih.gov/17068365/).
- Fogliata A, Vanetti E, Albers D, et al. On the dosimetric behaviour of photon dose calculation algorithms in the presence of simple geometric heterogeneities: comparison with Monte Carlo calculations. *Phys Med Biol*. 2007; 52(5): 1363–1385, doi: [10.1088/0031-9155/52/5/011](https://doi.org/10.1088/0031-9155/52/5/011), indexed in Pubmed: [17301460](https://pubmed.ncbi.nlm.nih.gov/17301460/).
- Soleymanifard S, Aledavood SA, Noghreiyani AV, et al. In vivo skin dose measurement in breast conformal radiotherapy. *Contemp Oncol (Pozn)*. 2016; 20(2): 137–140, doi: [10.5114/wo.2015.54396](https://doi.org/10.5114/wo.2015.54396), indexed in Pubmed: [27358592](https://pubmed.ncbi.nlm.nih.gov/27358592/).
- Schettini M, Maia M, Campos T. The development of an anthropomorphic and anthropometric thorax female phantom for experimental radiodosimetry. *Int J Low Radiation*. 2007; 4(2): 124, doi: [10.1504/ijlr.2007.015437](https://doi.org/10.1504/ijlr.2007.015437).
- Nogueira LB. Synthesis, Characterization and Dosimetry of Ho and HoZr Radioactive Seeds for Breast Cancer Treatment. UFMG, Belo Horizonte, Brazil 2012.
- Devic S, Tomic N, Lewis D. Reference radiochromic film dosimetry: Review of technical aspects. *Phys Med*. 2016; 32(4): 541–556, doi: [10.1016/j.ejmp.2016.02.008](https://doi.org/10.1016/j.ejmp.2016.02.008), indexed in Pubmed: [27020097](https://pubmed.ncbi.nlm.nih.gov/27020097/).
- Devic S, Seuntjens J, Sham E, et al. Precise radiochromic film dosimetry using a flat-bed document scanner. *Med Phys*. 2005; 32(7Part1): 2245–2253, doi: [10.1118/1.1929253](https://doi.org/10.1118/1.1929253), indexed in Pubmed: [28493574](https://pubmed.ncbi.nlm.nih.gov/28493574/).
- van Battum LJ, Hoffmans D, Piersma H, et al. Accurate dosimetry with GafChromic EBT film of a 6 MV photon beam in water: what level is achievable? *Med Phys*.

- 2008; 35(2): 704–716, doi: [10.1118/1.2828196](https://doi.org/10.1118/1.2828196), indexed in Pubmed: [18383692](https://pubmed.ncbi.nlm.nih.gov/18383692/).
22. Saur S, Frengen J. GafChromic EBT film dosimetry with flatbed CCD scanner: a novel background correction method and full dose uncertainty analysis. *Med Phys*. 2008; 35(7): 3094–3101, doi: [10.1118/1.2938522](https://doi.org/10.1118/1.2938522), indexed in Pubmed: [18697534](https://pubmed.ncbi.nlm.nih.gov/18697534/).
23. Xu LB. Commissioning of a GafChromic EBT Film Dosimetry Protocol at Ionizing Radiation Standards Group of National Research Council. . McGill University, Quebec 2009.
24. International Atomic Energy Agency. Absorbed dose determination in external beam radiotherapy: An International code of practice for dosimetry based on standards of absorbed dose to water. IAEA, Vienna 2000.
25. Cameron M, Cornelius I, Cutajar D, et al. Comparison of phantom materials for use in quality assurance of microbeam radiation therapy. *J Synchrotron Radiat*. 2017; 24(Pt 4): 866–876, doi: [10.1107/S1600577517005641](https://doi.org/10.1107/S1600577517005641), indexed in Pubmed: [28664894](https://pubmed.ncbi.nlm.nih.gov/28664894/).
26. Silva SD. Desenvolvimento de um fantoma de tórax e mama para comparações de protocolos de radioterapia mamária. Thesis, Nuclear Engineering Department, UFMG, Belo Horizonte, Brazil 2018.
27. ICRU. International Commission on Radiation Units and Measurements. Prescribing, Recording and Reporting Photon Beam Therapy — ICRU REPORT 50. ICRU, Maryland 1993.
28. Nogueira LB, Silva HL, de Campos TP. Experimental dosimetry in conformal breast teletherapy compared with the planning system. *Appl Radiat Isot*. 2015; 97: 93–100, doi: [10.1016/j.apradiso.2014.12.022](https://doi.org/10.1016/j.apradiso.2014.12.022), indexed in Pubmed: [25562678](https://pubmed.ncbi.nlm.nih.gov/25562678/).
29. Nogueira LB, Lemos SHL, Silva SD, et al. Skin Dosimetry in Breast Teletherapy on an Anthropomorphic and Anthropometric Phantom. *Austin J of Radiol* . 2015; 2(4): 1024.
30. Gershkevitch E, Schmidt R, Velez G, et al. Dosimetric verification of radiotherapy treatment planning systems: results of IAEA pilot study. *Radiother Oncol*. 2008; 89(3): 338–346, doi: [10.1016/j.radonc.2008.07.007](https://doi.org/10.1016/j.radonc.2008.07.007), indexed in Pubmed: [18701178](https://pubmed.ncbi.nlm.nih.gov/18701178/).
31. Aland T, Kairn T, Kenny J. Evaluation of a Gafchromic EBT2 film dosimetry system for radiotherapy quality assurance. *Australas Phys Eng Sci Med*. 2011; 34(2): 251–260, doi: [10.1007/s13246-011-0072-6](https://doi.org/10.1007/s13246-011-0072-6), indexed in Pubmed: [21465275](https://pubmed.ncbi.nlm.nih.gov/21465275/).